Available online at www.sciencedirect.com

ScienceDirect

Ceramics International 40 (2014) 3561–3569

CERAMICS INTERNATIONAL

www.elsevier.com/locate/ceramint

Transformation-assisted consolidation of Y_2O_3:Eu^{3+} nanospheres as a concept to optical nanograined ceramics

R.P. Yavetskiy[a,*], V.N. Baumer[a], M.I. Danylenko[b], A.G. Doroshenko[a], I.N. Ogorodnikov[c], I.A. Petrusha[d], A.V. Tolmachev[a], V.Z. Turkevich[d]

[a]*STC "Institute for Single Crystals", NAS of Ukraine, 60 Lenin Ave., 61001 Kharkov, Ukraine*
[b]*Frantsevich Institute for Problems of Materials Science, NAS of Ukraine, 3 Krzhizhanovsky Str., 03680 Kyiv, Ukraine*
[c]*Ural Federal University, 19 Mira Str., 620002 Yekaterinburg, Russia*
[d]*V.Bakul Institute for Superhard Materials, NAS of Ukraine, 2 Avtozavodskaya Str., 04074 Kyiv, Ukraine*

Received 18 July 2013; received in revised form 3 August 2013; accepted 16 September 2013
Available online 21 September 2013

Abstract

A concept is proposed to produce Y_2O_3:Eu^{3+} optical nanograined ceramics by the transformation-assisted consolidation of nanospheres under 8 GPa pressure. The nanoceramics were prepared by high-pressure low-temperature sintering ($\sim$0.04–0.2T_m, where T_m is the melting temperature) accompanied by the cubic-to-monoclinic phase transition. The effects of sintering conditions upon phase composition, grain size evolution, density, morphology, optical and luminescent properties of sintered ceramics have been studied. It has been shown that Y_2O_3:Eu^{3+} nanograined ceramics consisting of individual (cubic or monoclinic) phases or their mixture can be obtained by variation of the sintering temperature. The use of transformation-assisted consolidation makes it possible to prepare Y_2O_3:Eu^{3+} nanoceramics with average grain size three times smaller (12 nm) than that of the starting nanopowders (37 nm), which corresponds to extremely low grain growth factor of 0.3. The grain size refinement is related to numerous nucleation events in the parent phase of cubic yttrium oxide. The preparation conditions of translucent (T=50%) composite Y_2O_3:Eu^{3+} nanograined ceramics with a relative density of 99 $\pm$ 1 % have been determined. The obtained two-phase ceramics show high optical transparency due to negligible birefringence at extremely small ($\sim$12 nm) average grain size.

Keywords: A. Sintering; B. Grain size; C. Optical properties; D. Y_2O_3; Transformation-assisted consolidation

1. Introduction

Fabrication of novel optical ceramics with advanced properties required for future generations of optical devices is one of the most significant problems of modern materials science [1,2]. Yttrium sesquioxide Y_2O_3 (yttria) is not only a promising material for high-intensity discharge lamps and thermally stable windows, but also an excellent optical material for functional applications in photonics, optoelectronics, laser and scintillation techniques, etc. The thermal conductivity of yttria is much higher as compared with traditional $Y_3Al_5O_{12}$ laser crystals, which is favorable for laser application. However, obtaining of high-quality Y_2O_3 single crystals is extremely difficult because of high melting temperature ($\sim$2430 °C) and phase transition near the melting point [3]. Due to unique combination of physical and chemical properties (high corrosion resistance and thermal stability, optical transparency in the 0.17–6.5 μm wavelength range, high isomorphic capacity for introduction of luminescent ions, etc.), Y_2O_3 ceramics have a number of advantages as compared with single crystals. These advantages include wider range of compositions, improved mechanical properties and processability, lower cost of fabrication, etc. [4–7]. In comparison with micron-sized analogs, nanograined yttria ceramics (d < 100 nm) show much better mechanical properties [8]. In principle, they should also show better optical transparency due to negligibly weak light scattering on randomly oriented nanograins and pores of sizes considerably smaller than the visible light wavelength. However, obtaining pore-free transparent ceramics even with

*Corresponding author. Tel.: +380 57 3410415; fax: +380 57 3409343.
E-mail address: yavetskiy@isc.kharkov.ua (R.P. Yavetskiy).

0272-8842/$ - see front matter © 2013 Elsevier Ltd and Techna Group S.r.l. All rights reserved.
http://dx.doi.org/10.1016/j.ceramint.2013.09.072

cubic structure requires precise control of the phase and chemical composition and size limitation of the scattering centers at the nanoscale level [9].

Despite numerous publications on highly-transparent Y_2O_3 coarse-grained ceramics (e.g., [4,10] and references therein), only few works describe obtaining of dense Y_2O_3 nanostructured ceramics. However, no evidence of their transparency was presented. In [11,12] 99–99.6%-dense Y_2O_3 nanocrystalline ceramics was obtained by two-step sintering of nanopowders with average particle size of 10–30 nm; no data on their optical transparency were reported. Marder et al. reported preparation of Y_2O_3 samples by spark plasma sintering of nanocrystalline powders [13]. Consolidation of 17 nm nanopowders at rather high temperatures (1100 °C, or approximately $0.45T_m$) resulted in loss of the nanocrystalline character of ceramics. Y_2O_3 nanoceramics was also obtained by the high pressure-induced reversible phase transformation process [8], but despite high relative density of the sintered ceramics no transparency was achieved.

The transformation-assisted consolidation of nanopowders under high pressures is known to be an effective approach to manufacture oxide nanograined ceramics, with the process being accompanied by a decrease in specific volume [14–18]. The use of high pressures suppresses the diffusion mobility of the cations and, consequently, the grain growth rate, while the phase transformation promotes plastic flow of the material. The phase transition speeds up the diffusion–dislocation processes, which favor efficient consolidation of the ceramics due to rotation of the nanograins and their movement as a whole. The procedure allows one to obtain nanograined ceramics with a grain size even smaller than that of the starting powders, owing to higher nucleation rate of the transformed phase during sintering [16–18]. The method was applied to many oxide systems in high-pressure low-temperature sintering of their metastable nanopowders, with the aim of taking advantage of metastable-to-stable phase transformation for suppression of the grain growth. Thus, synthesis was reported of nanograined TiO_2 ceramics with grain size of 20–60 nm and density $>$ 97–99% [14,17,18], as well as 98.2% dense Al_2O_3 nanoceramics with grain size of 50 nm [19]; however, the required optical transparency was not achieved. Such an approach is not suitable for yttrium oxide, since the transition of the metastable monoclinic modification (B) into the stable cubic one (C) is accompanied by the specific volume increase by about 7%. In our previous paper [20], we reported Y_2O_3:Eu^{3+} nanograined optical ceramics manufactured by transformation-assisted consolidation of stable cubic nanopowders under high pressures. The present paper is aimed at more detailed analysis of the phase state, microstructure and optical properties of the nanograined yttria ceramics doped with europium ions.

2. Experimental

Y_2O_3:Eu^{3+} (1 at% europium) nanocrystalline spheres of cubic structure were obtained by the homogeneous chemical co-precipitation method according to [21]. Yttrium and europium nitrates were used as starting materials, and urea as a precipitant. The formed $Y(OH)CO_3 \cdot nH_2O$ precipitate was collected, filtered, repeatedly washed with water and ethyl alcohol and dried in air at $T=25$ °C. Then the powders were grinded and calcined at 800–1000 °C for 2 h. The particle size distribution was determined using a Zetasizer 1000HSA (Malvern Instruments, England) dynamic light scattering system. The consolidation of nanopowders was carried out by sintering under 8 GPa pressure in the 25–500 °C temperature range for 30–180 s using a toroid type high pressure (HP) apparatus [22]. Before placing in the HP cell, the initial nanopowders were uniaxially compacted under 250 MPa pressure into pellets with relative density of 50–55%.

The density of the consolidated samples was estimated by the standard Archimedes method. Phase identification was performed via the X-ray diffraction (XRD) method on a SIEMENS D-500 X-ray diffractometer (CuKα radiation, graphite monochromator) on the powdered ceramics samples. The phases were identified using JCPDS PDF-1 card file and EVA retrieval system included in the diffractometer software. The Rietveld refinement was performed with FullProf program [23]. The average apparent size of the crystallites was calculated with FullProf using a powder pattern of LaB_6 to obtain the instrumental profile function. The initial data on the monoclinic Y_2O_3 for the Rietveld refinement were taken from [24]. The microstructure of the ceramics was studied by high-resolution analytical transmission electron microscopy (HR TEM) using a JEM-2100F (JEOL) microscope equipped with an INCA (Oxford Instruments) X-ray microanalyzer. The samples for HR TEM were prepared by ion thinning. The optical measurements were performed on 1 mm thick ceramic plates with polished surfaces. The in-line optical transmittance of the samples was determined using a Perkin-Elmer "LAMBDA-35" spectrophotometer in 200–1000 nm wavelength range. The measurements of luminescence spectra at 10 K were carried out at the SUPERLUMI station of HASYLAB (Hamburg, Germany). The measurement technique and methods were described in detail in [25].

3. Results and discussion

3.1. Phase composition of Y_2O_3:Eu^{3+} nanograined ceramics

Transformation-assisted consolidation under high pressures requires phase-pure yttrium oxide nanopowders in the cubic form, since even small quantities of the metastable monoclinic phase in the starting nanocrystalline powders can substantially affect the densification efficiency [13]. However, yttrium oxide nanopowders possess polymorphism and crystallize into the monoclinic modification when the particle sizes are smaller than 7 ± 6 nm [26]. Y_2O_3:Eu^{3+} nanopowders were synthesized by the homogeneous co-precipitation method followed by calcination of an amorphous precursor to convert it into the crystalline state. The controlled conditions of precipitation and crystallization of yttria nanopowders make it possible to obtain particles of spherical morphology, low agglomeration degree and monodispersity. Fig. 1 presents the morphology and particle size distribution of spherical-shaped Y_2O_3:Eu^{3+}

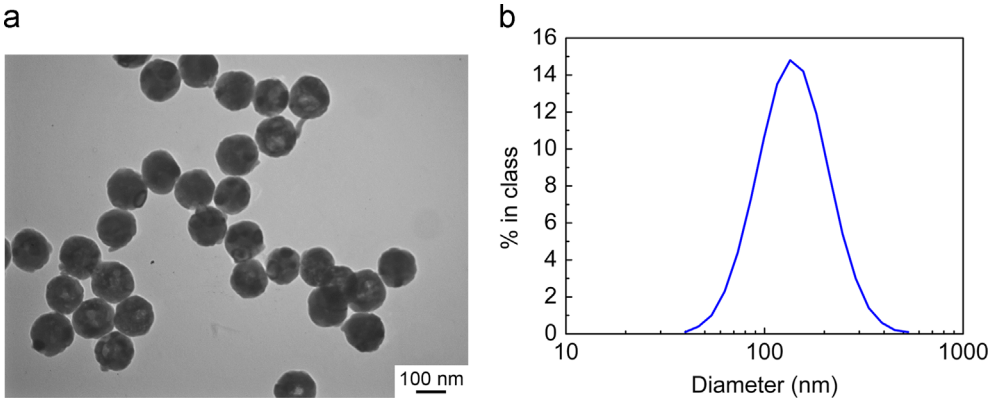

Fig. 1. TEM micrograph (1) and particles size distribution (2) of co-precipitated Y_2O_3:Eu^{3+} (1 at %) nanospheres calcined at 800 °C for 2 h.

(1 at%) nanopowders. The powders consist of spherical particles with an average particle size of 124 ± 10%, with each sphere formed by ~40 nm crystallites separated by nanoscale pores (Fig. 1a). This means that each nanosphere is polycrystalline. According to XPA data, the powder is characterized by 100% content of the cubic phase, the sp.gr. *Ia*3, $a=10.60402(14)$ Å, $V=1192.37(3)$ Å^3, the microstresses $\varepsilon=0.0095\%$. The lattice parameter of Y_2O_3:Eu^{3+} (1 at%) nanopowders is almost the same as that for pure Y_2O_3 ($a=10.600$ Å) due to nearly identical sizes of yttrium and europium cations of coordination number (CN) 6. The average crystallite size determined by the Rietveld method is 37.1 nm, i.e. it is approximately one-third of the diameter of the initial particle (124 nm), which confirms its polycrystallinity. Moreover, relatively large crystallite size of Y_2O_3 spheres provides crystallization of phase-pure stable cubic modification. Unlike particles of arbitrary morphologies, the spherical particles may be packed into compacts with a density of about 64 % which is close to random packing density of monodispersed spheres [27]. Moreover, polycrystalline particles possess higher sinterability in comparison with single-crystalline spheres of similar size [28].

After being compacted at ~250 MPa pressure, the obtained green bodies were consolidated under 8 GPa and subjected to X-ray phase analysis in order to determine influence of the sintering conditions on the structural-phase state of Y_2O_3:Eu^{3+} nanoceramics. Fig. 2 presents XRD patterns of Y_2O_3:Eu^{3+} nanograined ceramics as function of the consolidation temperature. We did not observe phase transition in Y_2O_3:Eu^{3+} spheres consolidated under 8 GPa at room temperature (Fig. 2). The obtained cubic ceramics were characterized by higher lattice parameters $a=10.6184(4)$ Å, $V=1197.23(8)$ Å^3, $\varepsilon=0.51\%$, probably due to elastic deformation of the nano-sized crystallites under high pressures. The partial transition into the metastable monoclinic modification starts at rather low temperature of 100 °C at 8 GPa, as shown by diffraction reflexes of the monoclinic yttria (Fig. 2). As the temperature rises, the intensity of peaks of the monoclinic phase increases while that of the cubic modification diminishes, and finally at 500 °C the $C\rightarrow B$ transformation is completed (Fig. 2). The bulk Y_2O_3 is known to undergo cubic-to-monoclinic phase transition starting in the 7.9–12 GPa pressure range [29–32]. Europium-doped Y_2O_3 is transformed into monoclinic modification under 7.9 GPa [31], which is close to the value obtained in our experiments. Unlike the previously reported improved compressibility of 20 nm Y_2O_3:Eu^{3+} nanocrystals up to 15 GPa [33], we observed the onset of $C\rightarrow B$ phase transition already at 8 GPa. This can be explained by the actual average pressure at the particle contacts being typically higher by a stress multiplication factor g ranging from 1 to 3 [18]. The polycrystalline yttria nanospheres already have a number of intercrystalline contacts within the individual sphere. These contacts represent boundaries between individual crystallites (characterized by increased defectivity level as interface states), so they can play the role of nucleation centers.

The cubic-to-monoclinic phase transformation of Y_2O_3 is a kind of so-called reconstructive transitions and is accompanied with substantial modification of the crystalline structure. In the cubic Y_2O_3 all the yttrium atoms are six-fold coordinated by oxygen atoms, while in the monoclinic unit cell yttrium atoms form YO_6 and YO_7 polyhedra in the ratio of 1:2. The lattice parameters of cubic and monoclinic Y_2O_3:Eu^{3+} slightly decrease with the consolidation temperature. In particular, B–Y_2O_3 obtained at 100 and 500 °C have the following lattice parameters: $a=14.026(5)$ $b=3.5188(10)$, $c=8.601(3)$ Å, $\beta=100.59(3)^\circ$, $V=417.3(3)$Å^3, $\varepsilon=1.7\%$ and $a=13.847(8)$, $b=3.506(2)$, $c=8.613(5)$ Å, $\beta=100.08(3)^\circ$, $V=411.75(4)$ Å^3, $\varepsilon=0.017\%$, respectively, which were found to be in a good agreement with the experimental and calculated data [34–36]. The temperature increase results in activation of diffusion processes and improvement of crystals structure. The volumes of the cubic and monoclinic Y_2O_3 per one formula unit are 74.63 and 69.55 Å^3, respectively. So, during $C\rightarrow B$ phase transformation the specific volume diminishes approximately by ~7% which favors the formation of dense ceramics. No texture was observed for composite ceramics, indicating the absence of preferred orientations of crystallites of monoclinic phase nucleated in the parent cubic yttria.

Fig. 3 presents quantitative X-ray phase analysis by the Rietveld method of Y_2O_3:Eu^{3+} nanograined ceramics. The phase transformation $C\rightarrow B$ starts at the temperatures below 100 °C and is virtually completed at 500 °C. The phase

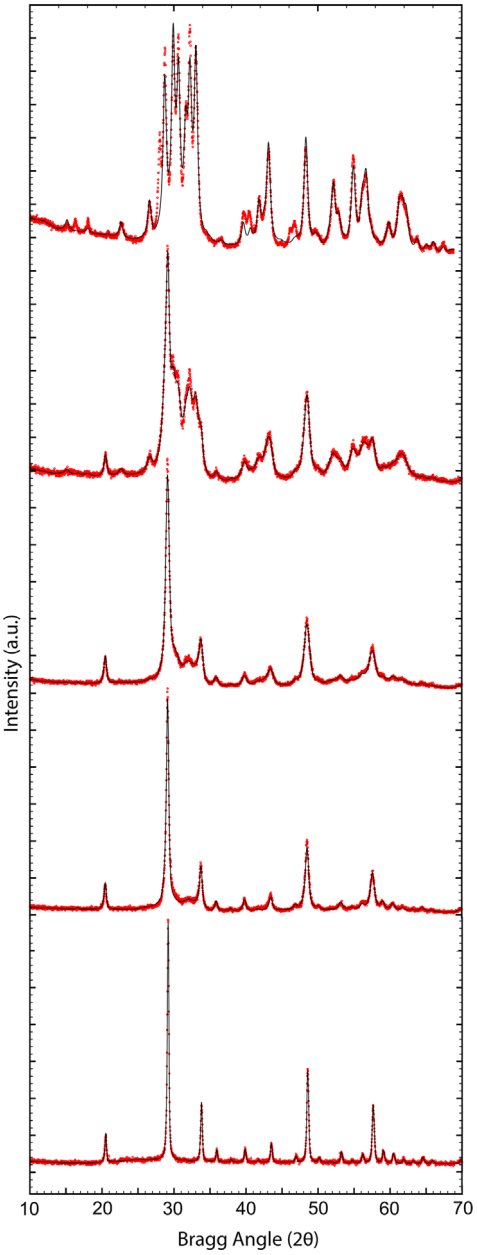

Fig. 2. Results of Rietveld refinement for Y_2O_3:Eu^{3+} (1 at%) nanopowders (1) and nanostructured ceramics obtained under 8 GPa and 25 (2), 100 (3), 300 (4) and 500 °C (5) for 30 s.

transition of the cubic yttria into the monoclinic modification is kinetically controlled [35], so the rise of sintering temperature results in an increase in the relative content of the monoclinic phase. $C \rightarrow B$ phase transition is irreversible, thus the high-pressure monoclinic phase persists in the sintered ceramics after decompression to ambient pressure. Even relatively low sintering temperatures of 100–500 °C ($\sim$0.04–0.2T_m) at 8 GPa pressure impose an additional driving force to the atoms which is high enough to overcome the pressure-induced potential barrier and to form nuclei of monoclinic phase due to enhanced atom diffusion [37]. The transformation rate is very high: approximately one-half of yttrium oxide is transformed into the monoclinic modification at 100 °C in only 30 s. Under

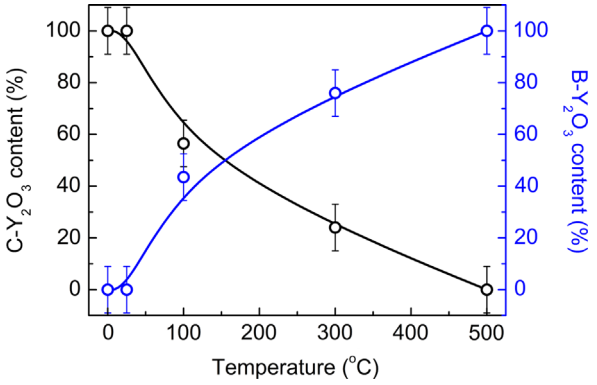

Fig. 3. Phase composition of Y_2O_3:Eu^{3+} (1 at%) nanograined ceramics sintered at 8 GPa for 30 s as function of the consolidation temperature.

the ambient conditions $B \rightarrow C$ reverse transition occurs at $T \sim 900$ °C [26] thus presenting the temperature limit of phase stability of the sintered composite yttria nanoceramics.

3.2. Grain sizes and densities of Y_2O_3:Eu^{3+} nanoceramics

The sintering temperature has an important effect on the grain size of Y_2O_3:Eu^{3+} composite nanoceramics, as shown in Fig. 4. The consolidation of nanopowders at room temperature is accompanied by a minor increase in the crystallite size from 37 to 44 nm, probably due to activation of surface diffusion during quasi-hydrostatic compression. However, this situation changes drastically at temperatures higher than a certain critical value when the formation of monoclinic yttria occurs. For example, at 300 °C the average grain size of both cubic (18 nm) and monoclinic Y_2O_3:Eu^{3+} (9 nm) is much smaller than that of initial nanopowders (37 nm) (Fig. 4a). This effect is related to numerous nucleation events in the parent phase of cubic yttrium oxide [18]. The grain size of the monoclinic yttria formed is practically independent on the sintering temperature and ranges between 9 and 12 nm, which is about 10 times larger than the lattice parameters (Fig. 4a). Low homologous sintering temperatures and high nucleation rate which seems to be higher than the growth rate are responsible for this effect. Fig. 4b summarizes the obtained results on the average crystallite size of Y_2O_3:Eu^{3+} nanoceramics; the values were calculated accounting for the specific weight of each phase (Fig. 3). Only consolidation at room temperature results in "coarse" nanoceramics (with average crystallite size somewhat higher than that of the initial nanopowders). The mean grain size of Y_2O_3:Eu^{3+} ceramics sintered in the 200–500 °C temperature range is only 12 nm, which corresponds to an unprecedented low grain growth factor of about 0.3, i.e., smaller than previously reported for TiO_2 nanoceramics ($\sim$0.5) [18]. Refinement of ceramics grain size down to 10–15 nm range may be caused by a decrease in the thermodynamic barrier for nucleation under high pressures, since consolidation is accompanied by irreversible decrease of the material's specific volume [16].

Production of optical nanoceramics implies preparation of a fully-dense material, i.e., pore-free ceramics. Fig. 5 shows

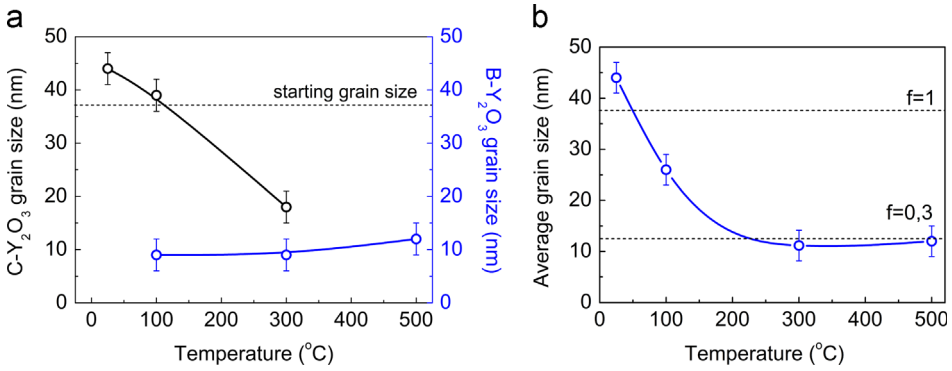

Fig. 4. Grain size (a) and the average grain size calculated taking into account the specific weight of each phase (b) of the cubic and monoclinic modification of Y_2O_3:Eu^{3+} (1 at%) as function of the consolidation temperature.

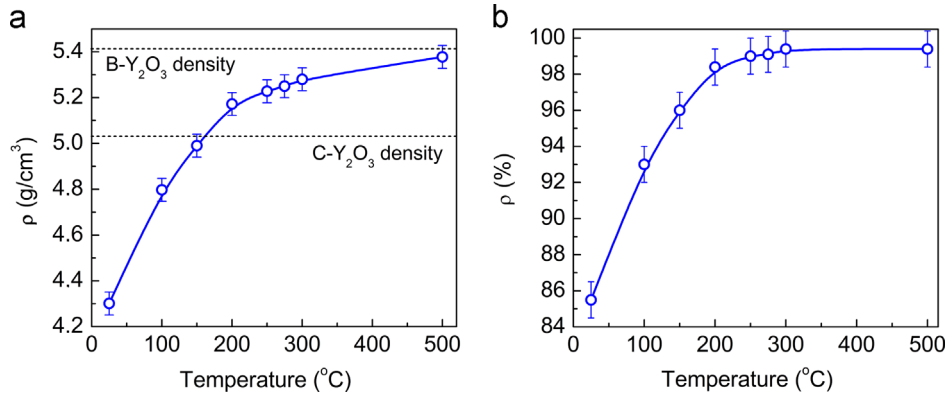

Fig. 5. Density (a) and relative density of Y_2O_3:Eu^{3+} (1 at%) nanograined ceramics calculated taking into account specific weight at each phase (b) as function of the consolidation temperature.

density of the formed ceramics as a function of the sintering temperature. Single-phase cubic Y_2O_3:Eu^{3+} ceramics consolidated at 25 °C densify up to 4.3 g/cm^3, corresponding to the relative density of 85 ± 1 % with respect to the theoretical value (5.03 g/cm^3). This value is much higher than random packing factor of spherical particles (64%) [27], indicating that a plastic deformation of monosized nanospheres occurs during consolidation at high pressure. Mesoporous structure of Y_2O_3:Eu^{3+} nanospheres consisting of 30–40 nm crystallites separated by nanometric pores is favorable for densification of ceramics even at room temperature due to facilitated movements of individual particles. The 85 ± 1% density of ceramics indicates that sintering is at an intermediate stage, since the lower limit for formation of closed porosity in rare-earth oxides is 95% [38]. Consequently, Y_2O_3:Eu^{3+} ceramics obtained under 8 GPa and 25 °C have large open pores and look opaque. The density of two-phase composite ceramics is essentially higher in comparison with monophase samples with cubic structure. Even at T=100 °C (which corresponds to 50% degree of phase transformation) the density reaches 4.8 g/cm^3 and tends to further increase with temperature. Fig. 5b presents the relative density of $(C+B)Y_2O_3$:Eu^{3+} nanoceramics as function of the consolidation temperature, calculated taking the phase composition into account (Fig. 3). In the optimal temperature range of 200–300 °C the density of the nanograined ceramics is intermediate between the theoretical values for the cubic (5.03 g/cm^3) and monoclinic Y_2O_3 (ρ=5.41 g/cm^3) and reaches 5.2–5.3 g/cm^3, which corresponds to 99 ± 1% relative density. Thus, transformation-assisted consolidation results in improved densification resulting from decreasing plastic flow resistance. Reconstruction of the crystal lattice allows activation of the compaction process by active motion of the particles as a whole, grain boundary sliding, as well as accommodation mechanisms or superplastic deformation of the polycrystalline material [39].

3.3. Optical and luminescent properties of Y_2O_3:Eu^{3+} nanoceramics

Fig. 6 presents the photographs of typical Y_2O_3:Eu^{3+} (1 at%) nanoceramics obtained by transformation-assisted consolidation. The phase-pure cubic nanograined ceramics are opaque because of large content of residual pores due to incomplete consolidation. Y_2O_3:Eu^{3+} nanoceramics obtained under the optimized barothermal conditions (P=8 GPa, T=200–300 °C) is translucent, so a text can be read through it. The samples obtained at 500 °C are opaque and have black color due to the presence of color centers generated by reduction conditions during high-pressure sintering. The same coloration was recently observed in RE_2O_3 (RE=Y, Sc, Lu) single crystals [3]. Though Y_2O_3:Eu^{3+} optical nanoceramics is of composite structure and contains both optically-isotropic (cubic) and anisotropic (monoclinic) phases,

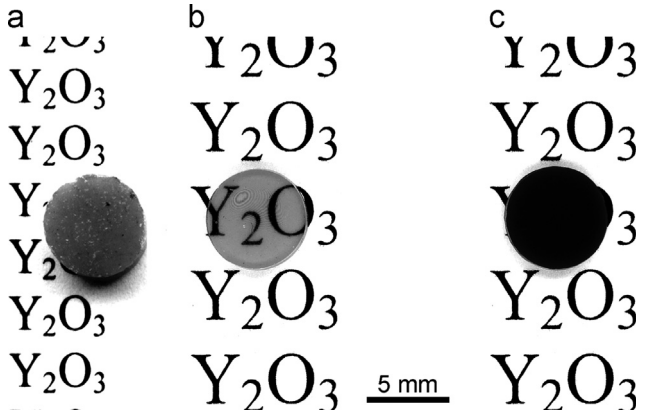

Fig. 6. Y_2O_3:Eu^{3+} (1 at%) nanograined ceramics obtained under 8 GPa pressure at T=25 (1), 200 (2) and 500 °C (3). The thickness of the tablets is 1 mm.

it is transparent. This results from low porosity of the samples obtained and negligible birefringence at extremely fine grain sizes (< 20 nm) [40]. So, only nanoceramics with the finest mean grain size of 12 nm (sintered at 200–300 °C) possess moderate transparency. Transformation-assisted consolidation of nanopowders under high pressures allows lowering of sintering temperatures required to obtain transparent yttria ceramics by one order of magnitude in comparison with the conventional method of vacuum sintering [4,10] due to increased driving force for consolidation induced by high pressure.

Fig. 7 presents the morphology of transparent Y_2O_3:Eu^{3+} nanoceramics containing both cubic and monoclinic modification of yttrium oxide in the ratio 40:60. The ceramics have nanocrystalline structure with grain size ranging from 10 to 30 nm, in agreement with XPA data (Fig. 3). Since the average grain size of the cubic yttria is larger as compared with the monoclinic modification, the 20 nm grains most probably correspond to the cubic yttrium oxide, whereas small grains (~10 nm) are of monoclinic modification (Fig. 7). According to high-resolution TEM data, no residual pores were observed in Y_2O_3:Eu^{3+} ceramics, suggesting almost complete densification. At the same time, the measured density of ceramics is still below the theoretical values, indicating the presence of residual porosity not revealed by HR TEM. Also, the aggregates of vacancies in the vicinities of the grain boundaries (which have lower densities in comparison with the bulk) may somewhat contribute to the residual porosity.

The transmission spectrum of Y_2O_3:Eu^{3+} composite nanoceramics is shown in Fig. 8. The in-line optical transmission of two-phase ceramics with 1 mm thickness reaches 50% at 900 nm. This is about 60% of the theoretical value for cubic Y_2O_3 single crystals (82.3%) calculated using data on dispersion of refraction index [41]. The transmission of ceramics as an optical medium is defined by many factors, such as the crystalline structure, porosity, pore sizes, the presence of optically active defects (color centers), etc. [42]. As a rule, optically isotropic materials with cubic crystal structure are favorable for preparation of optical ceramics due to absence of birefringence. At the same time, pore-free nanograined ceramics may also possess optical transparency due to changes in

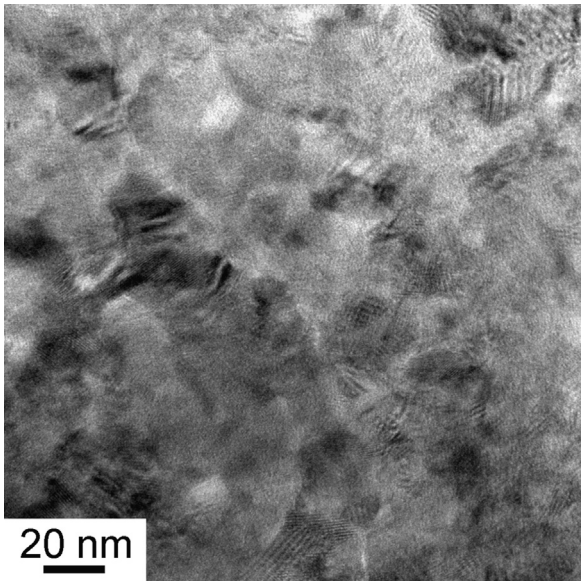

Fig. 7. HR TEM of Y_2O_3:Eu^{3+} (1 at%) nanoceramics sintered at 8 GPa and 200 °C for 30 s.

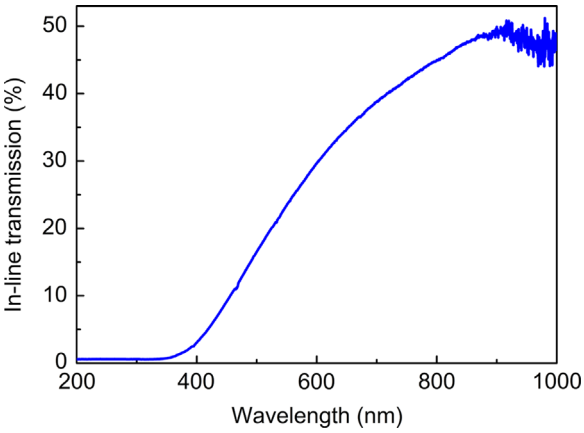

Fig. 8. In-line optical transmission spectrum for 1 mm-thick Y_2O_3:Eu^{3+} (1 at%) nanoceramics sintered at 8 GPa and 200 °C for 30 s.

the dominant scattering mechanism [9]. The optical properties of ceramics based on anisotropic materials may be improved by texture formation [43] or by the grain size refinement [40] when it is ensured that the porosity is negligible. Since no texture was observed in Y_2O_3:Eu^{3+} sintered composite ceramics, it seems that grain size refinement is responsible for the translucency achieved. According to theoretical calculation using the Mie scattering theory, a real in-line transmission of 50% in the visible light range is expected at 1 mm thickness and mean grain size < 40 nm, and 70% at the average grain size < 20 nm for fully dense tetragonal ZrO_2 ceramics [40]. Our calculations for yttria (to be published separately) give comparable value of mean grain size required to obtain the full transparency. So, other factors may contribute to the lower in-line transmission of Y_2O_3:Eu^{3+} nanoceramics in comparison with corresponding single crystals, namely, the residual porosity causing back-scattering of the incident light and absorption by color centers of unknown nature. To the best

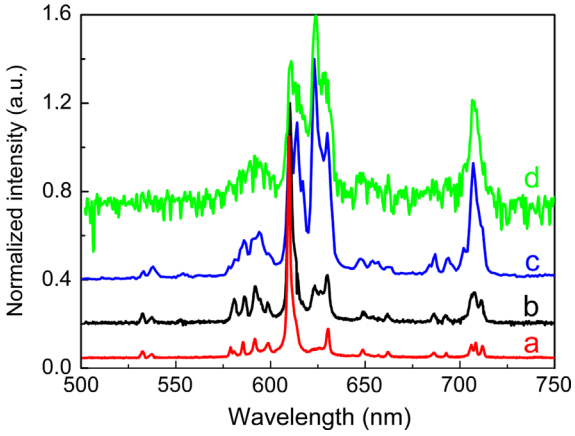

Fig. 9. VUV-luminescence spectra of Y_2O_3:Eu^{3+} (1 at%) nanospheres (a) and nanograined ceramics (b–d) measured at 10 K under excitation by synchrotron radiation at $\lambda = 204$ nm (a and b), 240 (c) and 323 nm (d).

of our knowledge, this is the first detailed report on translucent nanograined ceramics obtained by the transformation-assisted consolidation approach. Previous reports were focused on using the metastable-to stable phase transition to obtain nanograined ceramics with refined grain size, with no special interest in translucency (suggesting that the full densification was not achieved) [18]. To obtain dense nanograined ceramics, one requires not just metastable starting nanopowders, but the powders with the specific volume higher as compared to the nucleated phase. In the case of yttria, this is possible only with stable cubic phase.

Trivalent europium ions are excellent luminescent probes since their 4f–4f luminescence strongly depends on the crystallographic environment, crystal field symmetry and strength [33,44]. So, variation of CN of Eu^{3+} ions during the phase transition must be reflected in emission spectra. Fig. 9 presents low-temperature VUV luminescence spectra of cubic Y_2O_3:Eu^{3+} (1 at%) nanospheres and the most transparent two-phase nanoceramics. The luminescence of Y_2O_3:Eu^{3+} nanopowders with a maximum at $\lambda = 611$ nm is presented by well-known groups of the lines in the 500–720 nm wavelength range corresponding to $^5D_0 \rightarrow {}^7F_J$ ($J = 0$–4) transitions of europium ions (Fig. 9a) [45]. The luminescence is mainly due to transitions of Eu^{3+} ions located in the C_2 noncentrosymmetric site; the lines due to C_{3i} (S_6) symmetrical site are much weaker. Luminescence of Y_2O_3:Eu^{3+} composite nanograined ceramics is more complex and originates from Eu^{3+} emission in cubic (Fig. 9b) or monoclinic yttria (Fig. 9c), or from radiative transitions in europium ions occupying the "perturbed" positions (Fig. 9d). Luminescence spectra of nanoceramics strongly depend on the excitation wavelength. For example, excitation of nanoceramics into the Eu^{3+}–O^{2-} charge transfer band ($\lambda_{ex.} = 240$ nm) results in the luminescence of europium ions located mainly in monoclinic crystals (Fig. 9c). This luminescence has maxima at 615 and 624 nm corresponding to $^5D_0 \rightarrow {}^7F_2$ transitions of europium ions in monoclinic yttria. At a longer excitation wavelength ($\lambda = 323$ nm) the emission spectrum of Y_2O_3:Eu^{3+} nanoceramics is presented by wide broadened bands in the 575–630 nm and 700–725 nm wavelengths ranges. By analogy with Y_2O_3:Eu^{3+} nanocrystalline powders and nanostructures embedded in amorphous alumina, these bands were attributed to the europium ions occupying "perturbed" positions with disordered environment [46,47]. Most probably, perturbed sites of europium ions are located at the grain boundaries, taking into account fine grains size (10–15 nm) and large extension of grain boundaries in the sintered nanoceramics. Summarizing, the differences in the luminescence spectra of Y_2O_3:Eu^{3+} nanoceramics correspond to different crystalline environment of europium ions in the cubic (CN=6), monoclinic yttrium oxide (CN=6 and 7) and in perturbed sites near grain boundaries (CN $\approx$ 8) [47]. It is possible to excite quasi-selectively ions located either in the cubic phase or in the monoclinic phase or in perturbed sites at grain boundaries. More detailed studies of site-selective luminescence of Y_2O_3:Eu^{3+} composite nanoceramics are under way.

4. Conclusions

A concept to obtain Y_2O_3:Eu^{3+} (1 at%) optical nanograined ceramics via transformation-assisted consolidation of 125 ± 12 nm nanospheres at high pressure has been proposed. The process starts from nearly monodispersed low-agglomerated nanospheres of europium-doped yttria in stable cubic phase having higher specific volume as compared with that of high-pressure monoclinic modification. When nanospheres are subjected to sintering at 8 GPa and low homologous temperatures ($\sim$0.04–0.2 from melting temperature) the controlled cubic-to-monoclinic phase transition occurs resulting in fully-dense ($\rho = 99 \pm 1$ %) nanograined ceramics. It has been shown that consolidation temperature gives additional driving force to initiate phase transformation in the system at 8 GPa. Since cubic-to-monoclinic phase transition of yttria at high-pressures is irreversible, it is possible to adjust phase composition of sintered nanoceramics in the order C $\rightarrow$ C+B $\rightarrow$ B by increasing the consolidation temperature from 25 to 500 °C. High nucleation rate and low growth rate of monoclinic phase nucleated in the parent cubic yttria allowed us to obtain nanoceramics with unprecedentedly low average grain size of 12 nm, which is 3 times smaller than that of starting nanospheres (37 nm). This corresponds to grain growth factor of 0.3, the lowest value ever reported.

It has been determined that only Y_2O_3:Eu^{3+} composite nanoceramics with the finest mean grain size of 12 nm (sintered at 8 GPa and 200–300 °C) possess moderate optical transparency achieving 60% with respect to the corresponding single crystals. Translucency of Y_2O_3:Eu^{3+} nanoceramics containing both optically-isotropic (cubic) and anisotropic (monoclinic) phases may be caused by low residual porosity and negligible birefringence at extremely fine grain sizes. Trivalent europium ions act as a luminescent probe in composite Y_2O_3:Eu^{3+} nanograined ceramics since their 4f–4f luminescence strongly depends on the crystallographic environment. It is possible to excite quasi-selectively the ions located either in the cubic phase or in the monoclinic phase (or in perturbed sites at grain boundaries).

Acknowledgments

The authors are grateful for Yu.I. Pazura for peparation of starting nanopowders, O.M. Vovk and A.V. Ragulya for their help in characterization of powder samples and for V.A. Pustovarov for the help in VUV spectroscopy measurements. Authors from ISC, Kharkov, acknowledge support from Target Complex Program of Fundamental Research of NAS of Ukraine «Fundamental problems of Nanostructured Systems, Nanomaterials and Nanotechnologies» under the Project #78/13-N.

References

[1] J.-F. Li, W.-S. Liu, L.-D. Zhao, M. Zhou, High-performance nanostructured thermoelectric materials, NPG Asia Mater 2 (2010) 152–158.
[2] F. Maglia, I.G. Tredici, U. Anselmi-Tamburini, Densification and properties of bulk nanocrystalline functional ceramics with grain size below 50 nm, Journal of the European Ceramic Society 33 (2013) 1045–1066.
[3] R. Peters, K. Petermann, G. Hubert, Growth technology and laser properties of Yb-doped sesquioxides, in: P. Capper, P. Rudolph (Eds.), Crystal Growth Technology: Semiconductors and Dielectrics, Wiley-VCH Verlag GmbH & Co. KGaA, Weinheim, 2010, pp. 267–282.
[4] S.N. Bagayev, V.V. Osipov, M.G. Ivanov, V.I. Solomonov, V. V. Platonov, A.N. Orlov, A.V. Rasuleva, S.M. Vatnik, Fabrication and characteristics of neodymium-activated yttrium oxide optical ceramics, Optical Materials 31 (2009) 740–743.
[5] S.R. Podowitz, R. Gaume, R.S. Feigelson, Effect of europium concentration on densification of transparent Eu:Y_2O_3 scintillator ceramics using hot pressing, Journal of the American Ceramic Society 93 (2010) 82–88.
[6] M. Tokurakawa, A. Shirakawa, Ken-ichi Ueda, H. Yagi, T. Yanagitani, A.A. Kaminskii, K. Beil, C. Kränkel, G. Huber, Continuous wave and mode-locked Yb^{3+}:Y_2O_3 ceramic thin disk laser, Optics Express 20 (2012) 10847–10852.
[7] S.R. Podowitz, R. Gaume, R.S. Feigelson, Probing grain boundaries in ceramic scintillators using X-ray radioluminescence microscopy, Journal of Applied Physics 111 (013520) (2012) 12.
[8] B.H. Kear, J.F. Al-Sharab, R.K. Sadangi, S. Deutsch, N.B. Kavukcuoglu, S.D. Tse, A. Mann, O.A. Voronov, C.S. Nordahl, On the conversion of bulk polycrystalline Y_2O_3 into the nanocrystalline state, Journal of the American Ceramic Society 94 (2011) 1744–1746.
[9] G.L. Messing, A.J. Stevenson, Toward pore-free ceramics, Science 322 (2008) 383–384.
[10] L. Jin, G. Zhou, S. Shimai, J. Zhang, S. Wang, ZrO_2-doped Y_2O_3 transparent ceramics via slip casting and vacuum sintering, Journal of the European Ceramic Society 30 (2010) 2139–2143.
[11] I.-W. Chen, X.-H. Wang, Sintering dense nanocrystalline ceramics without final-stage grain growth, Nature 404 (2000) 168–171.
[12] X.-H. Wang, P.-L. Chen, I.-W. Chen, Two-step sintering of ceramics with constant grain-size, I. Y_2O_3, Journal of the American Ceramic Society 89 (2006) 431–437.
[13] R. Marder, R. Chaim, C. Estournes, Grain growth stagnation in fully dense nanocrystalline Y_2O_3 by spark plasma sintering, Materials Science and Engineering A 527 (2010) 1577–1585.
[14] K.-N.P. Kumar, K. Keizer, A.J. Burggraaf, T. Okubo, H. Nagamoto, S. Morooka, Densification of nanostructured titania assisted by a phase transformation, Nature 358 (1992) 48–51.
[15] S.-C. Liao, K.D. Pae, W.E Mayo, High pressure and low temperature sintering of bulk nanocrystalline TiO_2, Materials Science and Engineering A 204 (1995) 152–159.
[16] S.-C. Liao, K.D. Pae, W.E. Mayo, Retention of nanoscale grain size in bulk sintered materials via a pressure-induced phase transformation, Nanostructured Materials 8 (1997) 645–656.
[17] S.-C. Liao, W.E. Mayo, K.D. Pae, Theory of high pressure/low temperature sintering of bulk nanocrystalline TiO_2, Acta Materialia 45 (1997) 4027–4040.
[18] S.-C. Liao, J. Colaizzi, Y. Chen, B.H. Kear, W.E. Mayo, Refinement of nanoscale grain structure in bulk titania via a transformation-assisted consolidation (TAC) method, Journal of the American Ceramic Society 83 (2000) 2163–2169.
[19] B.H. Kear, J. Colaizzi, W.E. Mayo, S.-C. Liao, On the processing of nanocrystalline and nanocomposite ceramics, Scripta Materialia 44 (2001) 2065–2068.
[20] R.P. Yavetskiy, V.N. Baumer, N.A. Dulina, Yu.I. Pazura, I.A. Petrusha, V.N. Tkach, A.V. Tolmachev, V.Z. Turkevich, An approach to Y_2O_3:Eu^{3+} optical nanostructured ceramics, Journal of the European Ceramic Society 32 (2012) 257–260.
[21] Yu.I. Pazura, V.N. Baumer, T.G. Deyneka, O.M. Vovk, R.P. Yavetskiy, Synthesis of Y_2O_3 and Y_2O_3:Nd^{3+} monodisperse crystalline nanospheres by homogenous precipitation, Functional Materials 17 (2010) 107–113.
[22] L.G. Khvostantsev, L.F. Vereschagin, A.P. Novikov, Device of toroid type for high pressure generation, High Temperatures—High Pressures 9 (1977) 637–639.
[23] J. Rodriguez-Carvajal, T. Roisnel, FullProf.98 and WinPLOTR: new Windows 95/NT applications for diffraction commission for powder diffraction, IUCr Newsletter 20 (1998).
[24] B. Antič, M. Mitrič, D. Rodič, Cation ordering in cubic and monoclinic $(Y,Eu)_2O_3$: an X-ray powder diffraction and magnetic susceptibility study, Journal of Physics: Condensed Matter 9 (1997) 365–374.
[25] I.N. Ogorodnikov, V.A. Pustovarov, A.V. Tolmachev, R.P. Yavetskiy, Electronic excitation dynamics and energy transfer in lithium–gadolinium borates doped by rare earths, Physics of the Solid State 50 (2008) 1684–1686.
[26] P. Zhang, A. Navrotsky, B. Guo, I. Kennedy, A.N. Clark, C. Lesher, Q. Liu, Energetics of cubic and monoclinic yttrium oxide polymorphs: phase transitions, surface enthalpies, and stability at the nanoscale, The Journal of Physical Chemistry C 112 (2008) 932–938.
[27] R.K. Bordia, A theoretical analysis of random packing densities of monosized spheres in two and three dimensions, Scripta Metellurgica 18 (1984) 725–730.
[28] E.B. Slarnovich, F.F. Lange, Densification behavior of single-crystal and polycrystalline spherical particles of zirconia, Journal of the American Ceramic Society 73 (1990) 3368–3375.
[29] T. Atou, K. Kusaba, K. Fukuoka, M. Kikuchi, Y. Syono, Shock-induced phase transition of M_2O_3 (M=Sc, Y, Sm, Gd, and In)-type compounds, Journal of Solid State Chemistry 89 (1990) 378–384.
[30] E. Husson, C. Proust, P. Gillet, J.P. Itie, Phase transitions in yttrium oxide at high pressure studied by Raman spectroscopy, Materials Research Bulletin 34 (1999) 2085–2092.
[31] L. Wang, Y. Pan, Y. Ding, W. Yang, W.L. Mao, S.V. Sinogeikin, Y. Meng, G. Shen, H.-K. Mao, High-pressure induced phase transitions of Y_2O_3 and Y_2O_3:Eu^{3+}, Applied Physics Letters 94 (061921) (2009) 3.
[32] I. Halevy, R. Carmon, M.L. Winterrose, O. Yeheskel, E. Tiferet, S. Ghose, Pressure-induced structural phase transitions in Y_2O_3 sesquioxide, Journal of Physics: Conference Series 215 (012003) (2010) 8.
[33] X. Bai, H.W. Song, B.B. Liu, Y.Y. Hou, G.H. Pan, X.G. Ren, Effects of high pressure on the luminescent properties of nanocrystalline and bulk Y_2O_3:Eu^{3+}, Journal of Nanoscience and Nanotechnology, 8, 1404–1409.
[34] V. Srikanth, A. Sato, J. Yoshimoto, J.H. Kim, T. Ikegami, Synthesis and crystal structure study of Y_2O_3 high-pressure polymorph, Crystal Research and Technology 29 (1994) 981–984.
[35] H. Yusa, T. Tsuchiya, N. Sata, Y. Ohishiz, Dense yttria phase eclipsing the A-type sesquioxide structure: high-pressure experiments and *ab initio* calculations, Inorganic Chemistry 49 (2010) 4478–4485.
[36] P.P. Bose, M.K. Gupta, R. Mittal, S. Rols, S.N. Achary, A.K. Tyagi, S. L. Chaplot, Phase transitions and thermodynamic properties of yttria, Y_2O_3: inelastic neutron scattering shell model and first-principles calculations, Physical Review B 84 (094301) (2011) 11.
[37] K. Liu, D. He, H. Wang, T. Lu, F. Li, X. Zhou, High-pressure sintering mechanism of yttrium aluminum garnet ($Y_3Al_5O_{12}$) transparent nanoceramics, Scripta Materialia 66 (2012) 319–322.
[38] Z.M. Seeley, J.D. Kuntz, N.J. Cherepy, S.A. Payne, Transparent Lu_2O_3: Eu ceramics by sinter and HIP optimization, Optical Materials 33 (2011) 1721–1726.

[39] A.V. Ragulya, Consolidation of ceramic nanopowders, Advances in Applied Ceramics 107 (2008) 118–134.
[40] J. Klimke, M. Trunec, A. Krell, Transparent tetragonal yttria-stabilized zirconia ceramics: influence of scattering caused by birefringence, Journal of the American Ceramic Society 94 (2011) 1850–1858.
[41] Y. Nigara, Measurement of the optical constants of yttrium oxide, Japanese Journal of Applied Physics 7 (1968) 404–408.
[42] A. Krell, J. Klimke, T. Hutzler, Transparent compact ceramics: inherent physical issues, Optical Materials 31 (2009) 1144–1150.
[43] J. Akiyama, Y. Sato, T. Taira, Laser ceramics with rare-earth-doped anisotropic materials, Optics Letters 35 (2010) 3598–3600.
[44] D.K. Williams, B. Bihari, B.M. Tissue, J.M. McHale, Preparation and fluorescence spectroscopy of bulk monoclinic Eu^{3+}:Y_2O_3 and comparison to Eu^{3+}:Y_2O_3 nanocrystals, The Journal of Physical Chemistry B 102 (1998) 916–920.
[45] N.C. Chang, J.B. Gruber, Spectra and Energy Levels of Eu^{3+} in Y_2O_3, Journal of Chemical Physics 41 (3227) (1964) 8.
[46] W.W. Zhang, W.P. Zhang, P.B. Xie, M. Yin, H.T. Chen, L. Jing, Y. S. Zhang, L.R. Lou, S.D. Xia, Optical properties of nanocrystalline Y_2O_3: Eu depending on its odd structure, Journal of Colloid and Interface Science 262 (2003) 588–593.
[47] A. Pillonnet, J. Lancok, C. Martinet, O. Marty, J. Bellessa, C. Garapon, Structural and optical properties of Eu^{3+} doped Y_2O_3 nanostructures embedded in amorphous alumina waveguides prepared by pulsed laser deposition, Journal of Physics: Condensed Matter 18 (2006) 10043–10058.